

The Extreme Compact Starburst in MRK 273

C.L. Carilli and G.B. Taylor

NRAO, P.O. Box O, Socorro, NM, 87801, USA

Received _____; accepted _____

to appear in *Astrophysical Journal (letters)*

ABSTRACT

Images of neutral Hydrogen 21cm absorption and radio continuum emission at 1.4 GHz from Mrk 273 were made using the Very Long Baseline Array and Very Large Array. These images reveal a gas disk associated with the northern nuclear region with a diameter of $0.5''$ (370 pc), at an inclination angle of 53° . The radio continuum emission is composed of a diffuse component plus a number of compact sources. This morphology resembles those of nearby, lower luminosity starburst galaxies. These images provide strong support for the hypothesis that the luminosity of the northern source is dominated by an extreme compact starburst. The HI 21cm absorption shows an east-west gradient in velocity of 450 km s^{-1} across $0.3''$ (220 pc), implying an enclosed mass of $2 \times 10^9 M_\odot$, comparable to the molecular gas mass. The brightest of the compact sources may indicate radio emission from an active nucleus (AGN), but this source contributes only 3.8% to the total flux density of the northern nuclear region. The HI 21cm absorption toward the southeast radio nucleus suggests infall at 200 km s^{-1} on scales $\leq 40 \text{ pc}$, and the southwest near IR nucleus is not detected in high resolution radio continuum images.

Subject headings: galaxies:starburst, seyferts, active, ISM, individual:Mrk 273 - quasars:absorption lines - radio lines: galaxies - supernovae

1. Introduction

Luminous infrared galaxies are the most numerous sources with luminosities $\geq 10^{11} L_\odot$ in the nearby universe (Sanders and Mirabel 1996). The bulk of the luminosity from these sources is infrared emission from warm dust. A critical question concerning these sources is whether the dust is heated by an active nucleus, or a starburst? Recent studies using near IR spectroscopy suggest that the dominant dust heating mechanism in most luminous infrared galaxies (80%) is star formation (Genzel et al. 1998), although AGN heating may become significant for the highest luminosity sources ($\geq 10^{12.3} L_\odot$; Veilleux et al. 1999). This question has taken on new significance due to the recent discovery of a population of luminous infrared galaxies at high redshift seen in deep sub-millimeter and millimeter imaging surveys. If these high z sources are starbursts, then they may dominate the cosmic star formation rate at $z > 2$ (Smail, Ivison, and Blain 1997, Barger et al. 1998, Hughes et al. 1998, Blain et al. 1999, Eales et al. 1999, Bertoldi et al. 1999).

The most direct evidence to date of a dominant starburst in a luminous infrared galaxy is the discovery of a population of radio supernovae in the nuclear regions of Arp 220 by Smith et al. (1998) using high resolution imaging at 1.4 GHz. Radio observations are unique in this regard, since they are unobscured by dust and allow for imaging with mas resolution. We have begun a program of imaging the radio continuum emission and HI 21cm absorption in luminous infrared galaxies using the Very Long Baseline Array and the Very Large Array at resolutions ranging from 1 to 100 mas. Results on the Seyfert 1 galaxy Mrk 231 have been presented in Carilli, Wrobel, and Ulvestad (1998), Taylor et al. (1999), and Ulvestad, Carilli, and Wrobel (1998). Those data revealed the presence of an AGN driven radio-jet source on pc-scales at the center of a (possibly star forming) gas disk with a diameter of a few hundred pc, with about half the radio continuum emission coming from the disk.

In this letter we present the results on Mrk 273 at $z = 0.0377$. Mrk 273 has an infrared luminosity of $L_{\text{FIR}} = 1.3 \times 10^{12} L_{\odot}$ (as defined in Condon 1992), where we assume $H_o = 75 \text{ km s}^{-1} \text{ Mpc}^{-1}$. The optical galaxy has been classified as a Seyfert 2, LINER, and both (Baan et al. 1998, Colina, Arribas, and Borne 1999, Goldader et al. 1995), and it has a disturbed morphology on kpc-scales, with tidal tails indicating a merger event within the last 10^8 years (Knapen et al. 1998). Near IR spectroscopy reveals strong PAH features indicative of a starburst, but also high ionization lines indicative of an AGN (Genzel et al. 1998, Lutz et al. 1998). The X-ray emission also presents a mixed picture, with evidence for a highly absorbed hard component, but possible Fe L emission at 0.8 keV indicating cool (0.4 keV) gas (Iwasawa 1999). Broad absorption in the HI 21cm line and OH megamaser emission have also been detected in Mrk 273 (Baan, Haschick, and Schmelz 1985, Schmelz, Baan, and Haschick 1988).

The nuclear regions in Mrk 273 on sub-arcsecond scales are complex, with a double nucleus on a scale of $2''$ seen in the near IR (Knapen et al. 1998, Majewski et al. 1993, Armus et al. 1990), and in the radio continuum (Ulvestad and Wilson 1984, Condon et al. 1991, Knapen et al. 1998, Coles et al. 1999). The most peculiar aspect of Mrk 273 is that only one of the nuclei (the northern source) is seen in both the radio continuum and the near IR. The southeast nucleus is detected in the radio continuum, but is very faint in the near IR, although there may be a faint blue ‘star cluster’ at this position (Scoville et al. 2000). The southwest nucleus is seen in the near IR, but shows only very weak, extended radio continuum emission (Knapen et al. 1998). High resolution near IR imaging with the HST shows that both the north and southwest IR peaks are redder than the surrounding galaxy, and that the northern nucleus is redder than the southwestern nucleus (Scoville et al. 2000).

Imaging of CO emission from Mrk 273 shows a peak at the northern nucleus, with

faint extended emission on scales of a few arcseconds (Downes and Solomon 1998). Downes and Solomon derive a molecular gas mass of $1 \times 10^9 M_{\odot}$ for the northern nucleus, and find that the CO is most likely in a disk with size $< 0.6''$. From these data they conclude that the northern nucleus of Mrk 273 is an extreme compact starburst, with an IR luminosity of $6 \times 10^{11} L_{\odot}$ emitted from a region < 400 pc in diameter. This conclusion is supported by the $0.2''$ resolution images of the HI 21cm absorption presented in Coles et al. (1999), which reveal a velocity gradient along the major axis of the northern nucleus.

In this letter we present high resolution imaging (10 mas to 50 mas) of the HI 21cm absorption and radio continuum emission from Mrk 273. These data confirm the existence of a rotating gas disk with a diameter of 350 pc, and reveal a population of compact sources, possibly composed of luminous radio supernovae and/or nested radio supernova remnants.

2. Observations

Observations of Mrk 273 were made on May 31 and June 6, 1999 with the Very Long Baseline Array (VLBA), including the phased Very Large Array (VLA) as an element in the very long baseline array. The pass band was centered at the frequency of the neutral hydrogen 21cm line at a heliocentric redshift of: $z = 0.0377$, or $cz = 11300 \text{ km s}^{-1}$. The total bandwidth was 16 MHz, using two orthogonal polarizations, 256 spectral channels, and 2 bit correlation. The total on-source observing time was 13.4 hrs.

Data reduction was performed using the Astronomical Image Processing System (AIPS) and AIPS++. Standard *a priori* gain calibration was performed using the measured gains and system temperatures of each antenna. The compact radio source J1337+550 was observed every 5 minutes, and this source was used to determine the initial fringe rates and delays. The source 3C 345 was used to calibrate the frequency dependent gains (band pass

calibration). The source J1400+621 was used to check the absolute gain calibration. The results showed agreement of observed and expected flux densities to within 3%.

After application of the delay and rate solutions, and band pass calibration, a continuum data set for Mrk 273 was generated by averaging off-line channels. This continuum data set was then used for the hybrid imaging process, which involves iterative imaging and self-calibration of the antenna-based complex gains (Walker 1985). The final iteration involved both phase and amplitude calibration with a 3 minute averaging time for phases and 15 minutes for amplitudes. The self-calibration solutions were applied to the spectral line data set. The spectral line data were then analyzed at various spatial and spectral resolutions by tapering the visibility data, and by smoothing in frequency. The continuum emission was subtracted from the spectral line visibility data using UVLIN. Images of the line and continuum data were deconvolved using the Clark ‘CLEAN’ algorithm as implemented in IMAGR. For the radio continuum images we also employed the multi-resolution CLEAN algorithm as implemented in AIPS++ (Holdaway and Cornwell 1999). Results were consistent for all image reconstruction algorithms, and we present the naturally weighted Clark CLEAN continuum images in the analysis below. The full resolution of the naturally weighted images is 10 mas. We also present images at 50 mas resolution made using a Gaussian taper of the visibilities.

3. Results and Analysis

The 1.368 GHz continuum image of Mrk 273 at 50 mas resolution is displayed in Figure 1. The image shows that the northern nucleus is extended, with a major axis of $0.5''$ and a minor axis of $0.3''$. The region shows two peaks separated by $0.11''$. We designate the western peak N1 and the eastern peak N2. These two peaks can also be seen in near IR images of Mrk 273 (Knapen et al. 1998). The total flux density from this region is 86 ± 9

mJy. The southeastern source, which we designate SE, is also extended over about $0.3''$, with a total flux density of 40 ± 4 mJy.

Figure 2 shows the 1.368 GHz continuum images of the northern and southeastern nuclei of Mrk 273 at 10 mas resolution. The northern source is highly resolved, consisting of a diffuse component extending over $0.5''$, punctuated by a number of compact sources. Table 1 lists the positions and surface brightnesses at 10 mas resolution of the six sources with surface brightnesses ≥ 0.5 mJy beam $^{-1}$. Positions are relative to the peak surface brightness, corresponding to N1. The nominal position of N1 in Figure 2 is (J2000): $13^h44^m42.119^s$, $55^\circ53'13.48''$, based on phase-referencing observations using the celestial calibrator J1337+550 with a 5 minute cycle time. Note that the minimum error in the absolute astrometry is 12 mas, as set by the uncertainty in the calibrator source position (see Wilkinson et al. 1998 and references therein). The true error after phase transfer is likely to be significantly higher than this (Fomalont 1995, Beasley and Conway 1995).

Given the incomplete Fourier spacing coverage for VLBI imaging, in particular for short spacings, it is possible that the CLEAN algorithm has generated spurious point sources when trying to deconvolve extended emission regions. Conversely, we cannot rule-out the possibility that the extended emission is composed of mostly faint point sources. The use of multiresolution CLEAN mitigates these problems, and the sources listed in Table 1 all reproduce with essentially the same surface brightnesses for images made with the Clark CLEAN, multi-resolution CLEAN, and for images made with different visibility weighting schemes. The brightness temperatures of these sources are all $\geq 3 \times 10^6$ K, indicating non-thermal emission. The southeastern nucleus is also resolved, with high surface brightness emission occurring over a scale of 50 mas. We set a 4σ limit of 0.14 mJy to any compact radio source associated with the southwestern peak (large cross in Figure 1) seen at near IR wavelengths (Knapen et al. 1998).

Spectra of the HI 21cm absorption toward SE, and N1 and N2, at 50 mas resolution are shown in Figure 3. The spectrum of SE shows a double peaked profile, with the two lines separated by 400 km s^{-1} , each with a Full Width at Half Maximum (FWHM) of about 280 km s^{-1} . There is marginal evidence that each component has velocity sub-structure, but the SNR of these data are insufficient to make a firm conclusion on this point. The peak optical depth of each line is about 0.12 ± 0.02 , and the implied HI column density in each component is then: $N(\text{HI}) = 6.4 \pm 1.1 \times 10^{19} \times T_s \text{ cm}^{-2}$, where T_s is the HI spin temperature in K.

An interesting comparison is made with the MERLIN absorption spectra at $0.2''$ resolution toward the SE component (Coles et al. 1999). At this resolution, MERLIN detects 19 mJy of continuum emission, and shows a 3 mJy absorption line at about 11200 km s^{-1} , and weaker absorption of about 1 mJy at 11400 km s^{-1} . The VLBA data show a peak continuum surface brightness of 10 mJy beam^{-1} at 50 mas resolution, and absorption line depths of 1 mJy at both velocities. This suggests that the absorption at 11200 km s^{-1} is due to extended gas covering both the compact and extended continuum emitting regions, while the 11400 km s^{-1} absorption is due to a small cloud ($\leq 40 \text{ pc}$) covering only the high surface brightness continuum emission. Assuming 11200 km s^{-1} indicates the systemic velocity of the gas at that location in the galaxy disk (Coles et al. 1999), then the higher velocity system would be infalling at 200 km s^{-1} .

The spectrum of N2 shows a relatively narrow absorption line, with a $\text{FWHM} = 160 \text{ km s}^{-1}$, a peak optical depth of 0.59 ± 0.06 , and an HI column density of $1.8 \pm 0.2 \times 10^{20} \times T_s \text{ cm}^{-2}$. The spectrum of N1 shows a broad, flat absorption profile with $\text{FWHM} = 540 \text{ km s}^{-1}$, with optical depths ranging from 0.1 and 0.4 ± 0.04 across the line profile. Again, there is marginal evidence for a few narrower, higher optical depth components. The total HI column density is $1.8 \pm 0.3 \times 10^{20} \times T_s \text{ cm}^{-2}$. The velocity range of the HI absorption

toward N1 is comparable to that seen for the OH megamaser emission (Baan, Haschick, and Schmeltz 1985, Stavely-Smith et al. 1987).

Figure 4 shows the position-velocity (P-V) diagram for the HI 21cm absorption along the major axis of the northern nucleus. There is a velocity gradient from east to west of about 450 km s^{-1} across 300 mas, plus an apparent flattening of the velocity distribution to larger radii. The P-V distribution is confused somewhat by the broad absorption seen toward N1 (at position -90 mas in Figure 4). The east-west velocity gradient of the HI absorption across the northern source is consistent with results from MERLIN HI 21cm imaging at $0.2''$ resolution (Coles et al. 1999), and with the velocity field derived from CO emission observations at $0.6''$ resolution (Downes and Solomon 1998).

4. Discussion

The most significant result from our high resolution radio continuum imaging of Mrk 273 is that the emission from the northern nucleus extends over a region of $0.3'' \times 0.5''$ ($220 \times 370 \text{ pc}$), punctuated by a number of compact sources with flux densities between 0.5 and 3 mJy. This morphology resembles those of the starburst nuclei of NGC 253 and M82 (Ulvestad and Antonucci 1997, Muxlow et al. 1994), on a similar spatial scale. However, the total radio luminosity is an order magnitude larger in Mrk 273. The physical conditions in this region are extreme, with a minimum pressure of $10^{-9} \text{ dynes cm}^{-2}$, and corresponding magnetic fields of $100 \mu\text{G}$.

The 1.4 GHz radio continuum emission from nuclear starburst galaxies is thought to be primarily synchrotron radiation from relativistic electrons spiraling in interstellar magnetic fields, with the electrons being accelerated in supernova remnant shocks (Condon 1992, Duric 1988). The compact sources are then individual supernovae or supernova remnants,

while the diffuse emission is thought to be from electrons that have diffused away from the supernova remnant shocks. Our high resolution images provide strong support for the hypothesis of Downes and Solomon (1998) that the northern nucleus of Mrk 273 is an extreme compact starburst, with a massive star formation rate of $60 \text{ M}_\odot \text{ year}^{-1}$, as derived from the radio continuum luminosity (Condon 1992), and occurring in a region of only 370 pc diameter. From their detailed analysis of the CO emission from Mrk 273, Downes and Solomon (1998) propose that the star formation occurs in a disk with scale height of 21 pc and a total gas mass of $1 \times 10^9 \text{ M}_\odot$.

The nature of the weak, compact radio continuum sources in Mrk 273 is not clear, but given the similarity in morphology with the starburst nuclei in M82 and NGC 253, it is likely that these sources are a combination of nested supernova remnants and/or luminous radio supernovae. These sources have radio spectral luminosities $\geq 10^{28} \text{ ergs s}^{-1} \text{ Hz}^{-1}$ at 1.4 GHz, which is an order of magnitude higher than the brightest radio supernovae remnants seen in M82 (Muxlow et al. 1994), and are comparable in luminosity to the rare class of extreme luminosity radio supernovae characterized by SNe 1986J (Rupen et al. 1987) and 1979C (Weiler and Sramek 1988). A substantial population of such luminous supernovae has been discovered in the starburst nucleus of Arp 220 by Smith et al. (1998), who suggest that the high luminosities of those supernovae may indicate a denser local environment relative to typical supernovae, by a factor 3 or so (Chevalier 1984). If the compact sources in Mrk 273 are nested supernova remnants, then it would require 10 or more of the most luminous M82-type supernova remnants in regions less than 7 pc in size. Future high resolution imaging of Mrk 273 is required to clarify the nature of these compact sources.

It is possible that the brightest of the compact sources, coincident with N1, indicates the presence of a weak radio AGN. Supporting evidence for this conclusion is the broad HI absorption line observed toward N1. This component contributes only 3.8% to the total

radio luminosity at 1.4 GHz of the northern nuclear regions.

From flattening of the radio spectrum between 1.6 and 5 GHz, Knapen et al. (1998) suggested that there may be a dominant, synchrotron self-absorbed radio-loud AGN in the northern nucleus of Mrk 273. The images presented herein clearly preclude this hypothesis. We feel a more likely explanation for the low frequency flattening is free-free absorption. We are currently analyzing images with sub-arcsecond resolution between 327 MHz and 22 GHz in order to determine the origin of this low frequency flattening.

The gas disk hypothesis for the northern nucleus of Mrk 273 is supported by the observed velocity gradient in the HI 21cm absorption along the major axis. The rotational velocity at a radius of 220 pc is 280 km s^{-1} , assuming an inclination angle of 53° . Assuming Keplerian rotation, the enclosed mass inside this radius is then $2 \times 10^9 \text{ M}_\odot$, comparable to the molecular gas mass observed on this scale.

Overall, these data support the idea that the dominant energy source in the northern nuclear region in Mrk 273 is a starburst and not an AGN. However, the presence of an AGN somewhere in the inner $2''$ of Mrk 273 is still suggested, based on the high ionization near IR lines (Genzel et al. 1998), the (possible) hard X-ray component (Iwasawa 1999), and the Seyfert II optical spectrum, although Condon et al. (1991) argue that a Seyfert II spectrum is not necessarily a conclusive AGN indicator. It is possible that the AGN is located at either the SE radio nucleus, or the SW near IR nucleus.

The SE radio nucleus presents a number of peculiarities, the most important of which is the weakness of the near IR emission (Knapen et al. 1998, Scoville et al. 2000). Knapen et al. (1998) suggested that this source may simply be the chance projection of a background radio source. However, the probability of a chance projection of a 40 mJy source within $1''$ of the northern nucleus is only 4×10^{-7} (Langston et al. 1990, Richards et al. 1999). This low probability, and the fact that we see evidence for gas infall into the SE nucleus in the HI

21cm absorption images, effectively preclude the background source hypothesis. The radio morphology is consistent with an amorphous jet, or a very compact starburst, although the lack of CO emission from this region argues for an AGN. One possible cause for the lack of near IR emission is that the active region is still obscured at $2.2 \mu\text{m}$. The HI 21cm absorption column density is $6.4 \pm 1.1 \times 10^{22} \times (\frac{T_s}{10^3 \text{K}}) \text{ cm}^{-2}$, while the absorption column derived from the hard X-ray spectrum may be as large as $4 \times 10^{23} \text{ cm}^{-2}$, depending on the X-ray powerlaw index. Using the HI 21cm column leads to $A_v = 40 \times (\frac{T_s}{10^3 \text{K}})$, assuming a Galactic dust-to-gas ratio. This is comparable the extinction responsible for the obscuration in the near IR of the AGN in the powerful radio galaxy Cygnus A (Ward 1996). Imaging at wavelengths of $10 \mu\text{m}$ or longer, with sub-arcsecond resolution, is required to address this interesting question.

We do not detect any high surface brightness radio emission associated with the SW near IR nucleus. This could simply mean that this region harbours a radio quiet AGN. An alternative possibility is that this is a star forming region in which the star formation is very recent, commencing less than 10^6 years ago, such that a substantial population of radio supernovae and supernova remnants have not yet had time to develop.

We thank J. Wrobel, J. Ulvestad, and K. Menten for useful discussions and comments. This research made use of the NASA/IPAC Extragalactic Data Base (NED) which is operated by the Jet propulsion Lab, Caltech, under contract with NASA. The VLA and VLBA are operated by the National Radio Astronomy Observatory, which is a facility of the National Science Foundation operated under cooperative agreement by Associated Universities, Inc. CLC acknowledges support from the Alexander von Humboldt Society, and the Max Planck Institute for Radio Astronomy.

References

Armus, L., Heckman, T.M., and Miley, G.K. 1990, *ApJ*, 364, 471

Baan, W.A., Haschick, A.D., and Schmelz, J.T 1985, *ApJ* (letters), 298, 51

Baan, W.A., Salzer, J.J., and Lewinter, R.D. 1998, *ApJ*, 509, 633

Beasley, A.J. and Conway, J.E. 1995, in *Very Long Baseline Interferometry*, eds. J. Zensus, P. Diamond, and P. Napier, p. 327

Bertoldi, F. et al. 1999, *A&A* (letters), in preparation

Blain, A., Smail, I., Ivison, R.J., & Kneib, J.-P. 1999, *MNRAS*, 302, 623

Chevalier, R.A. 1984, *ApJ* (letters), 285, 63

Coles, G.H., Pedlar, A., Holloway, A.J., and Mundell, C.G. 1999, *MNRAS*, 310, 1033

Colina, L., Arribas, S., and Borne, K.D. 1999, *ApJ* (letters), 527, 13

Condon, J.J. 1992, *ARA&A*, 30, 575

Condon, J.J., Huang, Z.P., Yin, Q.F., and Thuan, T.X. 1991, *ApJ* 378, 65

Downes, D. and Solomon, P. 1998, *ApJ*, 507, 615

Duric, Neb 1988, *Space Science Reviews*, 48, 73

Iwasawa, K. 1999, *MNRAS*, 302, 961

Eales, S., et al. 1999, *ApJ*, 515, 518

Fomalont, E. 1995, in *Very Long Baseline Interferometry*, eds. J. Zensus, P. Diamond, and P. Napier, p. 363

Genzel, R. et al. 1998, *ApJ*, 498, 579

Goldader, J.D., Joseph, R.D., Doyon, R., and Sanders, D.B. 1995, *ApJ*, 444, 97

Holdaway, M. and Cornwell, T. 1999, in preparation

Hughes, D. et al. 1998, *Nature*, 394, 341

Knapen, J.H. et al. 1998, *ApJ* (letters), 490, 29

Langston, G.I., Conner, S.R., Hefflin, M.B., Lehar, J., and Burke, B.F. 1990, *ApJ*, 353, 34

Lutz, D., Spoon, H.W., Rigopoulou, D., Moorwood, A.F., and Genzel, R. 1998, *ApJ* (letters), 505, 103

Majewski, S.R., Hereld, M., Koo, D.C., Illingworth, G.D., and Heckman, T.M. 1993, *ApJ*, 402, 125

Muxlow, T.W., Pedlar, A., Wilkinson, P.N., Axon, D.J., Sanders, E.M., and de Bruyn, A.G. 1994, *MNRAS*, 266, 455

Richards, E. 1999, *ApJ*, in press

Rupen, M.P., van Gorkom, J.H., Knapp, G.R., Gunn, J.E., and Schneider, D.P. 1987, *AJ*, 94, 61

Sanders, D.B. and Mirabel, I.F. 1996, *ARAA*, 34, 749

Schmelz, J.T., Baan, W.A., and Haschick, A.D. 1988, *ApJ*, 329, 142

Scoville, N.Z. et al. 2000, *AJ*, in press (astroph 9912246)

Smail, I., Ivison, R., & Blain, A. 1997, *ApJ* (letters), 490, 5

Smith, H.E., Lonsdale, C.J., Lonsdale, C.J., and Diamond, P.J. 1998, *ApJ* (letters), 493, 17

Stavely-Smith, L., Cohen, R.J., Chapman, J.M., Pointon, L., and Unger, S.W. 1987, MNRAS, 226, 689

Taylor, G.B., Silver, C.S., Ulvestad, J.S., and Carilli, C.L. 1999, ApJ, 519, 185

Ulvestad, J.S., Wrobel, J.M., and Carilli, C.L. 1999, ApJ, 516, 127

Ulvestad, J.S. and Antonucci, R.J. 1997, ApJ, 488, 621

Ulvestad, J.S. and Wilson, A.S. 1984, ApJ, 278, 544

Veilleux, S., Sanders, D.B., and Kim, D.-C. 1999, ApJ, 522, 113

Walker, R.C. 1985, in Aperture Synthesis in Radio Astronomy, eds. R. Perley, F. Schwab, and A. Bridle (NRAO: Green Bank), p. 189

Ward, M.J. 1996, in *Cygnus A*, eds. C. Carilli and D. Harris, (Cambridge University Press), p. 43

Weiler, K.W. and Sramek, R.A. 1988, ARAA, 26, 295

Wilkinson, P.N., Browne, I.W.A., Patnaik, A.R., Wrobel, J.M., and Sorathia, B. 1998, MNRAS, 300, 790

Figure Captions

Figure 1 – An image of Mrk 273 at 1.368 GHz at 50 mas (37 pc) resolution. The contour levels are a geometric progression in the square root of two, hence every two contours implies a factor two rise in surface brightness. The first contour level is $0.25 \text{ mJy beam}^{-1}$. The peak surface brightness is 10 mJy beam^{-1} and the off-source rms is $85 \mu\text{Jy beam}^{-1}$. The reference position (0,0) corresponds to (J2000): $13^h44^m42.142^s$, $55^\circ53'13.15''$, based on phase-referencing observations using the celestial calibrator J1337+550 with a 5 minute cycle time. The cross in the SW corner indicates the position of the SW near IR nucleus.

Figure 2a – An image of the northern nuclear regions of Mrk 273 at 1.368 GHz at 10 mas (7.3 pc) resolution. The contours are linear with an increment of $0.1 \text{ mJy beam}^{-1}$, starting at $0.1 \text{ mJy beam}^{-1}$. The peak surface brightness is $3.05 \text{ mJy beam}^{-1}$ and the off-source rms is $36 \mu\text{Jy beam}^{-1}$.

Figure 2b – The same as Figure 2A, but now for the southeastern nuclear regions. The peak surface brightness is $1.35 \text{ mJy beam}^{-1}$.

Figure 3 – The HI 21cm absorption spectra toward Mrk 273 from images at 50 mas resolution. Figure 3a is the spectrum of N1. The peak surface brightness of $7.8 \text{ mJy beam}^{-1}$ has been subtracted. Figure 3b is the spectrum of N2. The peak surface brightness of $6.7 \text{ mJy beam}^{-1}$ has been subtracted. Both these spectra have a velocity resolution of 29 km s^{-1} . Figure 3c is the spectrum of SE at a velocity resolution of 58 km s^{-1} . The peak surface brightness of 10 mJy beam^{-1} has been subtracted. The zero point on the velocity scale corresponds to a heliocentric velocity of 11300 km s^{-1} in all spectra.

Figure 4 – The position-velocity plot for the HI 21cm absorption across the major axis of the northern nucleus of Mrk 273 at a spatial resolution of 50 mas (37 pc) and a velocity resolution of 60 km s^{-1} . The contour levels (in absorption) are: 0.4, 0.8, 1.2, 1.6, 2.0, 2.4, 2.8

mJy beam^{−1}. The position of continuum component N1 corresponds to −90 mas, while N2 corresponds to +20 mas. The zero point on the velocity scale corresponds to a heliocentric velocity of 11300 km s^{−1} in all spectra.

Table 1. Compact Sources in Mrk 273

Surface Brightness mJy beam ⁻¹	Relative Position mas
3.07	0 0
0.91	85E, 37N
0.76	75E, 14N
0.55	26E, 16S
0.53	110E, 33N
0.51	47W, 39S

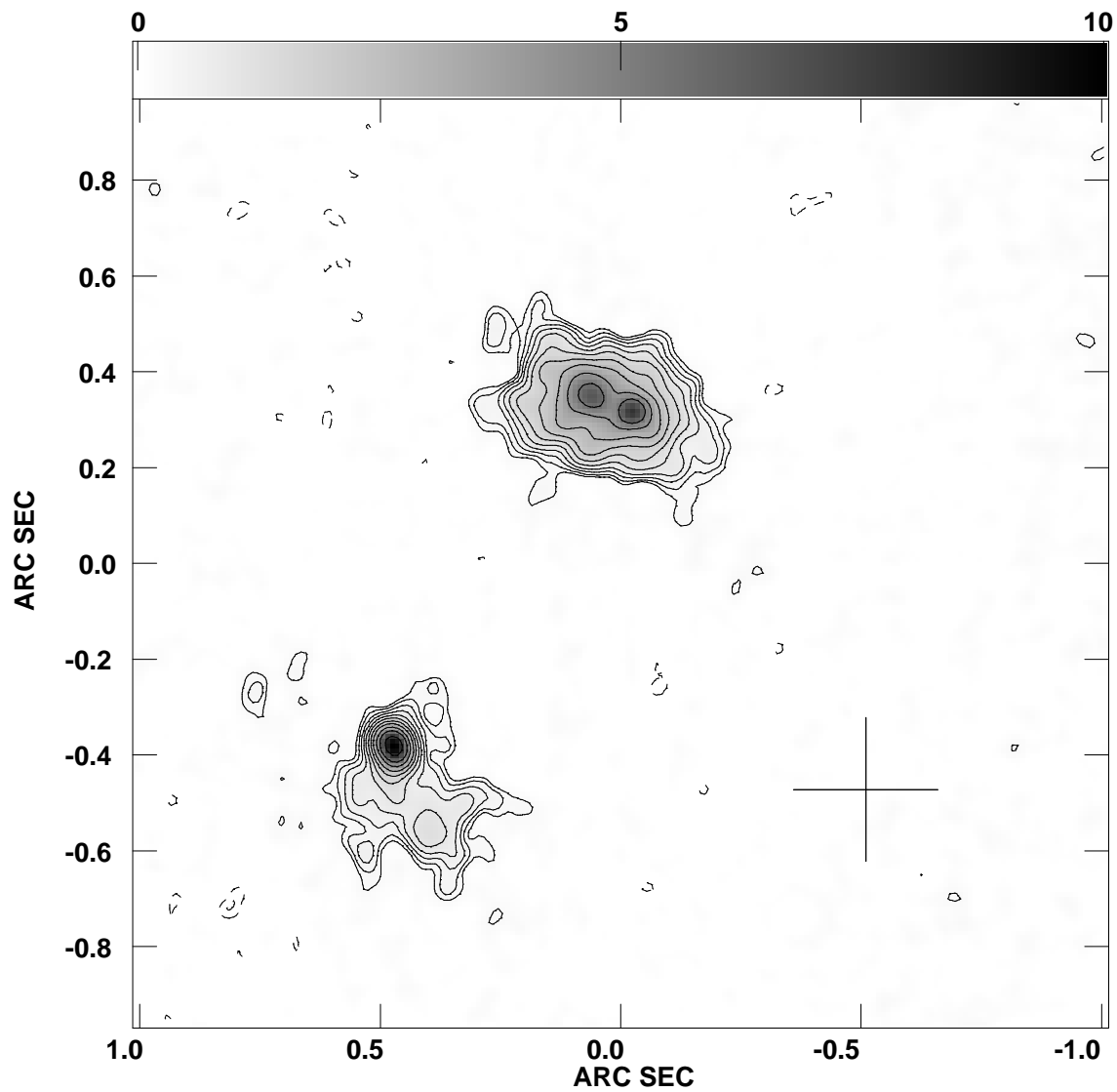


Fig. 1.—

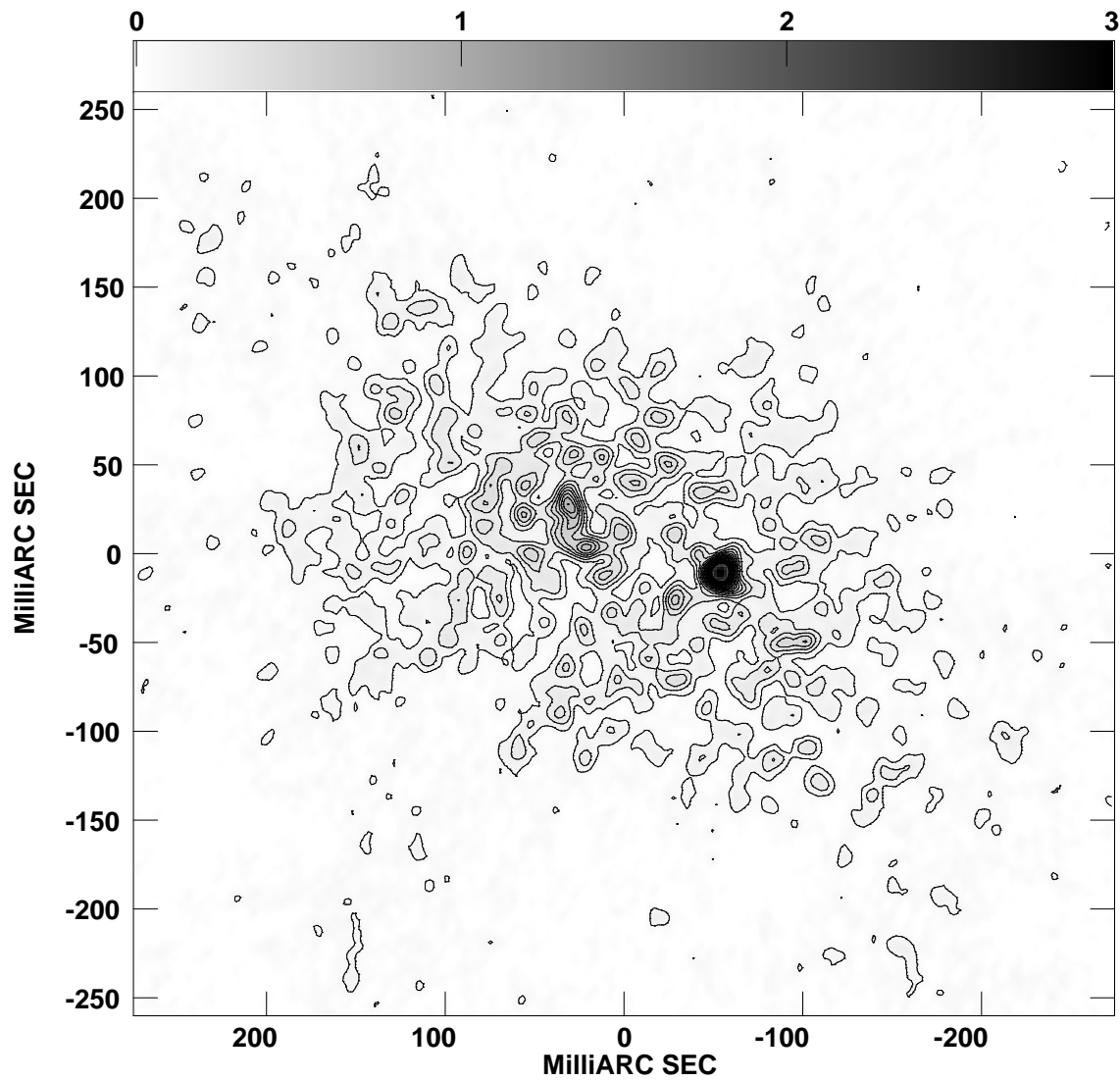
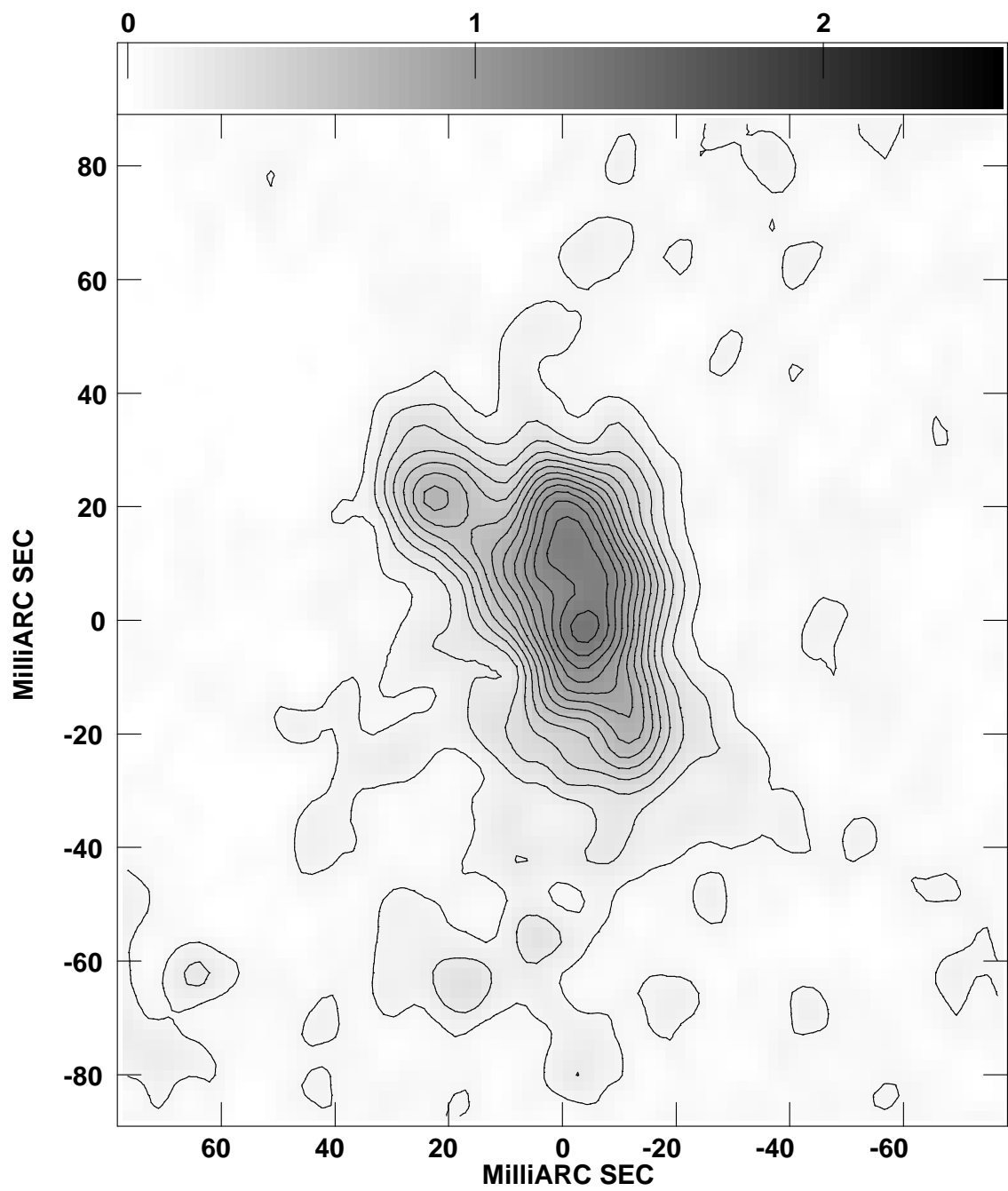
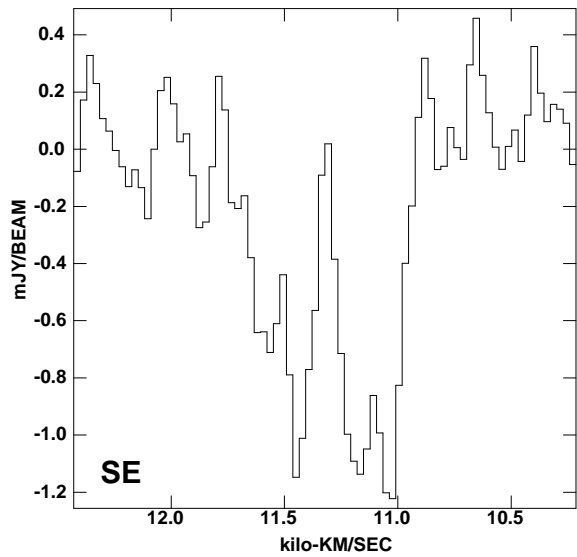
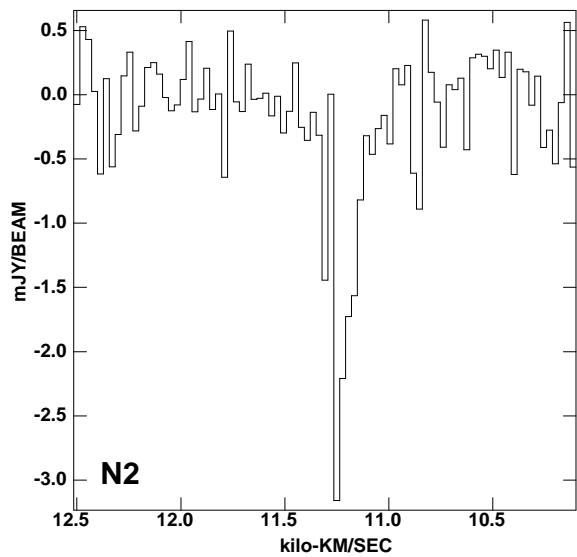
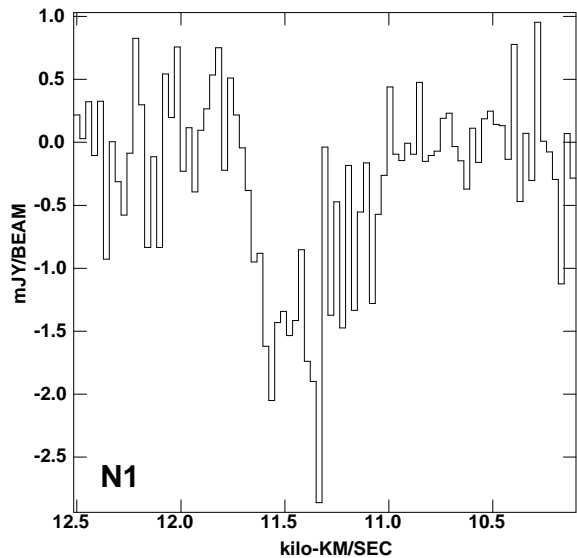


Fig. 2.—





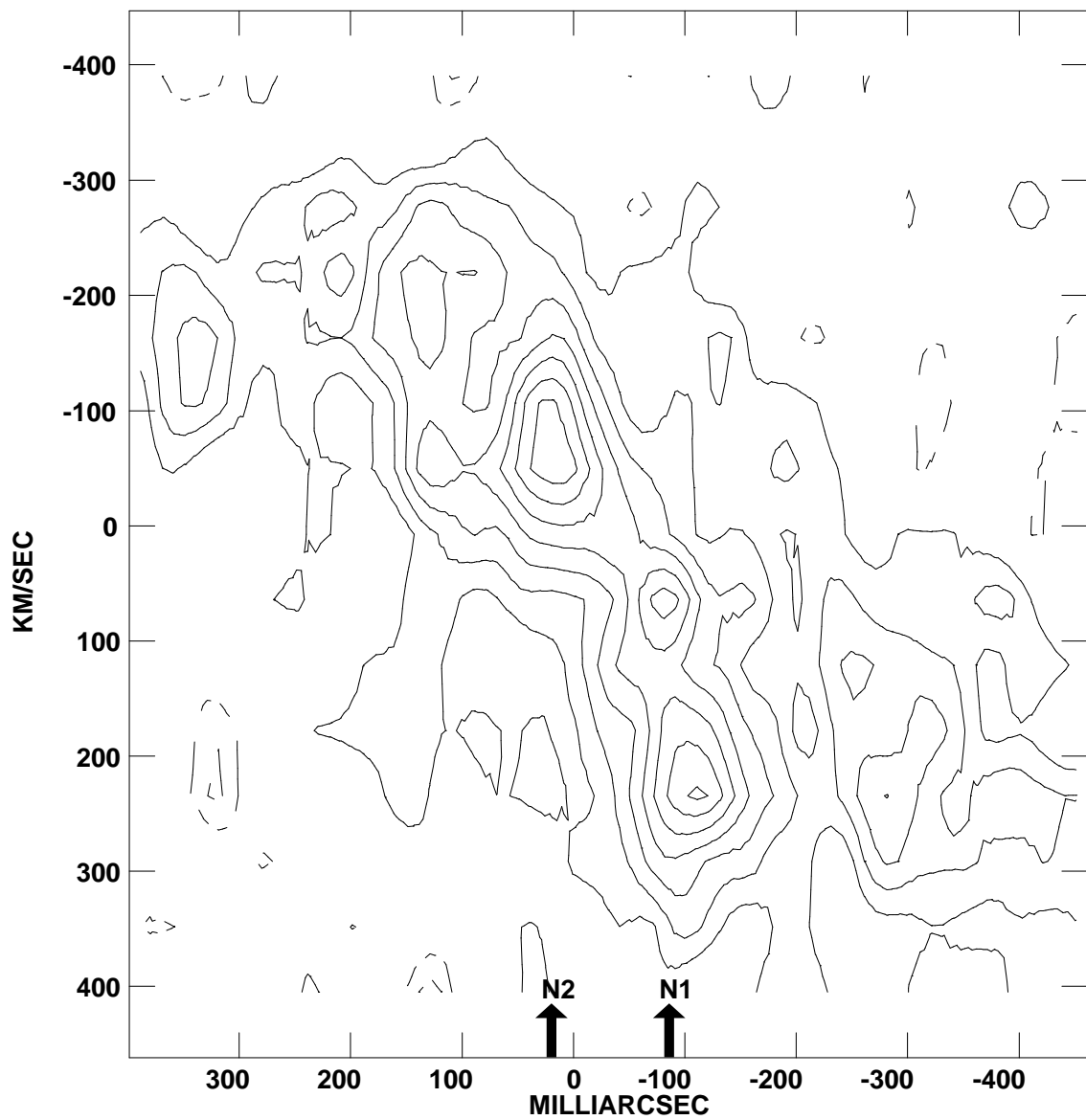


Fig. 4.—